J Appl Physiol 112: 1600–1611, 2012.
First published January 26, 2012; doi:10.1152/japplphysiol.01251.2011.

A biomechanical model for encoding joint dynamics: applications to transfemoral prosthesis control

Chris A. McGibbon

Institute of Biomedical Engineering and Faculty of Kinesiology, University of New Brunswick, Fredericton, New Brunswick, Canada

Submitted 6 October 2011; accepted in final form 23 January 2012

McGibbon CA. A biomechanical model for encoding joint dynamics: applications to transfemoral prosthesis control. *J Appl Physiol* 112: 1600–1611, 2012. First published January 26, 2012; doi:10.1152/japplphysiol.01251.2011.—This paper presents and tests a framework for encoding joint dynamics into energy states using kinematic and kinetic knee joint sensor data and demonstrates how to use this information to predict the future energy state (torque and velocity requirements) of the joint without a priori knowledge of the activity sequence. The intended application is for enhancing micro-controlled prosthetics by making use of the embedded sensory potential of artificial limbs and classical mechanical principles of a prosthetic joint to report instantaneous energy state and most probable next energy state. When applied to the knee during preferred and fast speed walking in 8 human subjects (66 preferred-speed trials and 50 fast-speed trials), it was found that joint energy states could be consistently sequenced (75% consensus) according to mechanical energy transference conditions and subsequences appeared to reflect the stability and energy dissipation requirements of the knee during gait. When simple constraints were applied to the energy transfer input conditions (their signs), simulations indicated that it was possible to predict the future energy state with an accuracy of >80% when 2% cycle in advance (~20 ms) of the switch and >60% for 4% (~40 ms) in advance. This study justifies future research to explore whether this encoding algorithm can be used to identify submodes of other human activity that are relevant to TFP control, such as chair and stair activities and their transitions from walking, as well as unexpected perturbations.

biomechanics; energy; gait

What are the Effects of Transfemoral Amputation on Mobility and Health?

Amputation of the lower extremity above the knee represents a significant mobility challenge (6, 8). Control of gait requires coordination of bilateral ankle, knee, and hip joints to provide adequate support and propulsion while ensuring safe and efficient locomotion (14, 19, 51). Loss of musculoskeletal and neurological function due to amputation impairs the central nervous system's ability to ensure safe and efficient locomotion, and although current prosthetic solutions can restore gross function for the amputee they cannot replicate the sensory function of the joint tissues and passive/active controls of the muscles of the person's limb prior to amputation.

Transfemoral amputees experience increased incidence of back pain (45) and higher risk of falls (44, 62) compared with nonamputee controls, even among those who routinely use transfemoral prostheses (TFP). Older amputees are also at increased risk of mobility complications due to existing chronic conditions such as diabetes and vascular disease (21).

What Advances Have Been Made in Restoring Function for TFP Users?

Over the last few decades, advancement in TFP design has shown great promise for the restoration of walking in the transfemoral amputee (23, 36). Commercially available TFP solutions consist mainly of mechanical systems that use locking mechanisms and dashpots to enable stance and swing phase control, respectively, during gait. These devices require the user to adapt to the mechanical constraints of the locking and damping mechanisms, which often results in gait abnormalities that reduce the efficiency of walking.

Although still cost prohibitive, micro-computer controlled TFPs enable the prosthesis and user to adapt simultaneously, via sensors that control stance and swing phase motion of the prosthesis and better meet the demands of the user. Several studies have documented the improvement in gait and walking function when using micro-controlled prostheses compared with mechanically controlled devices (31, 32, 37, 55). A more efficient and symmetrical gait (32, 48, 53, 55), better stair descent ability (31), and better balance (31) have been observed in TFP users with micro-controlled devices compared with users with mechanically controlled devices.

According to a recent study by the Research Department of Otto Bock (7), all the micro-controlled TFP currently available on the market (Otto Bock's C-Leg, Nabtesco's Hybrid Knee, Össur's Rheo Knee, and the Adaptive 2 from Chas A Blanchford & Son, UK) operate safely and efficiently for level, ramp, and stair walking, with very few differences between them for stance and swing control (7). Although ambulation is clearly a functional milestone for a transfemoral amputee, there remains a considerable need for more intelligent TFP technology to enable full mobility and the freedom to interact with the environment efficiently and safely (25).

What Are the Limitations that Prevent Restoring Full Mobility in TFP Users?

A significant issue with any micro-controlled device—be it upper or lower extremity—is resolving the user's intent so the appropriate motor commands can be issued by the controller. Electromyography (EMG) is the preferred approach for a number of reasons: muscle EMG is readily available from the amputee's residual limb and socket interface and the user can be trained to activate these muscles to cause the prosthesis to perform specific motions (29, 46, 56). Likewise, by using

Address for reprint requests and other correspondence: C. A. McGibbon, PhD. Univ. of New Brunswick, Institute of Biomedical Engineering, 25 Dineen Drive, Fredericton, New Brunswick, Canada E3B 5A3 (e-mail: cmcgibb@unb.ca).

discriminant models and classifiers, a prosthesis controller can be trained to recognize these specific patterns of muscle activity and identify the user's intent (26, 27). The technology has enjoyed significant success in the upper-extremity field of prosthetics in which restoration of volitional control is the goal. There has also been some recent success in applying this concept to volitional knee flexion control of the TFP knee while sitting (22).

It is recognized, however, that restoring locomotor activities in the transfemoral amputee presents a different set of challenges than those for upper extremity or volitional motions of the knee while sitting. Incorrect controller decisions while the user is carrying out an ambulatory task could result in an injurious fall. Ecological locomotor behavior in humans is rarely characterized as movement along a straight clear pathway. Many locomotor tasks involve transitions between different types of movement (28). For healthy limbed individuals, stops, turns, transitions from sitting to standing to walking, and vice versa, are typically performed in one fluid motion because the brain already knows the motor commands required to produce them. Transfemoral amputation clearly impacts the ability to achieve fluid motion while executing locomotor tasks of daily living (15).

What Are the Motor Control Implications for TFP Users?

For the natural human knee, the brain and spinal cord can monitor and respond to the joint's motion and loading environment via soft tissue mechanoreceptors and muscle spindles. Although it is still largely unknown how the brain and spinal cord encode movement, it is thought to be related to the biomechanical state of the joint, specifically the joint kinematics and kinetics (16). Animal studies have identified the interpositus nucleus as the potential source of this encoding, and evidence strongly suggests that an internal model of the limb's kinematics and dynamics are used in controlling extremity movements (9).This would suggest that a loss of kinematic and kinetic information below the amputation will require central nervous system (CNS) adaptation. Whether an amputee uses a mechanical or micro-controlled TFP, the tactile sensory organs in the residual limb alone are not sufficient to provide the CNS with information to control the artificial limb (49). TFP designs must therefore be overconstrained to prevent unwanted motions, and the user must be able to adapt to these constraints, often at the cost of efficiency.

However, the mechanical structure of artificial joints offers considerable potential for monitoring the physical environment of the "joint" and contributing to controller decisions. As with upper-extremity myoelectric prostheses, TFPs can incorporate sensory hardware for measuring biological signals (muscle EMG) and a variety of mechanical signals from the prosthesis, such as torque and angular position and/or speed. Although signals representing these quantities are presently used in experimental TFP designs as inputs to pattern recognition algorithms (12, 57), these designs do not take advantage of the fact that biomechanical relationships among these metrics can also reveal the energy state of the joint. It is argued below that prosthetic controllers could benefit from the ability to monitor and control energy states of the dynamic joint.

How Can Knowledge in Gait Biomechanics Improve TFP Control?

Prior research into human gait analysis provides a solid foundation for extending the sensory capabilities of TFP controller design to include information about the energy state of the joint. Although Elftman (18) described analysis of human joint power in the late 1930s, applications of energy, work, and power did not appear in rehabilitation biomechanics research until the 1980s with the pioneering work of Winter and colleagues (50, 58, 59, 61). Subsequently joint power and energy concepts were applied heavily throughout the 1990s and 2000s in gait research of young and old adults (13, 19, 30, 33, 34, 51, 60) and pediatric populations (10, 43, 47, 52, 54, 63). Most of these studies were focused on examining peak or average powers during various portions of gait rather than the transfer of energy between segments.

Robertson and Winter (50) published the first study related to energy generation, absorption, and transference during gait, followed by Aleshinsky (1–5) who published a very extensive treatise on the topic. These studies were limited to two-dimensional motion capture data, but were later applied to three-dimensional movement data by McGibbon et al. (38–42) to better understand gait compensations in disabled elders. This body of work suggests that segmenting a joint's dynamic time history into modes of possible energy states may be a useful way to analyze and understand how mobility adaptations occur. The present study applies this existing framework to address some of the above limitations that prevent achieving full mobility among TFP users.

What Are the Guiding Research Questions/Hypotheses of This Research?

The goal of this research is to improve the ability of future TFP users to achieve their full mobility capacity. The hypothesis is that simple measurements of the kinematics and kinetics of two articulating segments, such as those that comprise the TFP knee, a thigh and a shank segment, can be used to reveal the patterns of energy transfer through the mechanical joint and its actuator. Because there is a finite number of ways energy can be transferred across a joint, it may be possible to encode joint motions as energy transfer modes (5). Furthermore, because energy transfers follow a logically defined sequence, the prediction of future energy modes may also be possible. The implications of this theory have not been previously explored.

By simulating the capacity of TFP devices to provide sensory information relevant to the biomechanical principles of human movement control, this paper derives and tests a model for simple encoding of the current and future energy requirements of the prosthetic joint. To test this new concept, this paper uses gait data from able-bodied older adults to simulate how a set of simple knee joint sensors could be used to encode joint dynamics into energy states and how future energy states might be predicted.

MATERIALS AND METHODS

To demonstrate the principles of this encoding method, gait data were analyzed for eight able-bodied adult women over 65 yr of age performing repeated gait trials at self-selected normal and fast walking speeds. The study was reviewed and approved by University Research Ethics Board, and all participants provided written informed

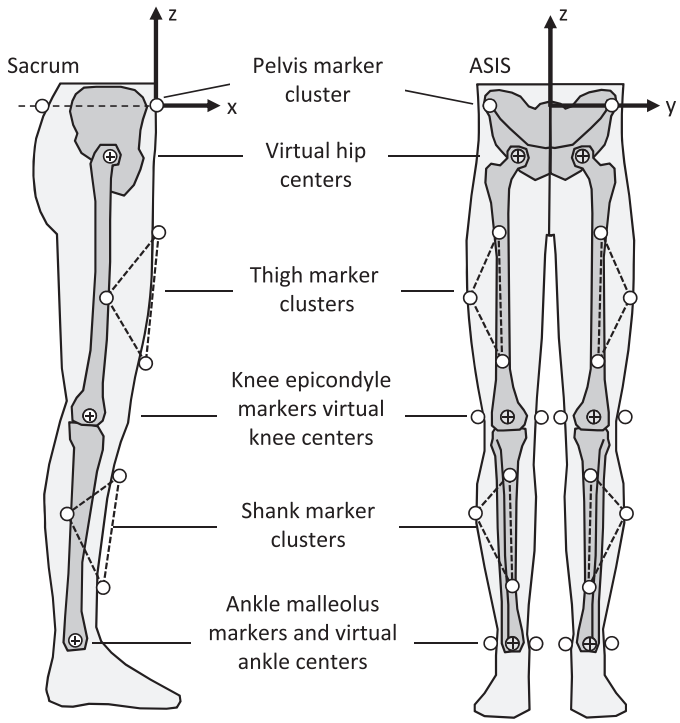

Fig. 1. Motion analysis markers consisted of 3 pelvis markers (sacrum, left ASIS, and right ASIS) and 3 thigh markers (superior, inferior, and lateral) and 3 shank markers (superior, inferior, and lateral) for left and right legs. The marker triads form clusters to represent pelvis, thigh, and shank segments. The knee joint was represented by markers at the medial and lateral epicondyle of the femur and the ankle with markers at the medial and lateral maleoli. Joint markers were required only for static standing trials. Marker clusters also used but not shown include the torso (left and right acromium processes and sternum) and feet (medial and lateral metatarso-phalangeal joints and great toe).

consent. This older group was selected on the basis of future planned research that focuses on geriatric amputees. They reported having no musculoskeletal or neurological disorders affecting locomotion. Gait data were collected at the UNB Institute of Biomedical Engineering, Motion Analysis Laboratory (calibrated xyz volume $4 \times 2 \times 2$), using an eight-camera Vicon MCam system and four (2×2 arrangement) Kistler force plates. Custom written Matlab (MathWorks) routines were used to process the kinematic and kinetic data.

Gait Analysis Protocol

Participants were first dressed in shorts and t-shirts and prepared for motion analysis by attaching markers to body segments using double-sided tape at anatomical locations shown in Fig. 1. Although only lower extremity data were used in the present analysis, foot, shank, thigh, pelvis, and torso data collected the present study only concerns the knee joint and, therefore, Fig. 1 shows only the markers relevant to computing thigh and shank (and knee) kinematics but describes the full marker set in the figure legend. During all trials, kinematic data were acquired at 60 Hz and force plate data at 1,500 Hz.

Three-dimensional joint kinematics were determined by first using a static standing trial to define marker clusters (on thigh and shank) and joint centers of the ankle knee and hip. As shown in Fig. 1, joint marker pairs on the ankle (medial and lateral malleoli) and knee (medial and lateral epicondyles) were used to define ankle and knee joint centers, and hip centers were estimated using pelvis (ASIS) markers and the algorithm of Davis et al. (11). Clusters on the thigh and shank were referenced to their respective embedded anatomical axes using a quaternion kinematic solver (20). Thigh and shank clusters tracked during walking trials were then used to compute shank and thigh anatomical angles and the relative knee flexion angle.

Walking trials were performed at each participant's self-selected normal walking speed and fast-as-possible walking speed. Up to 10 trials at each speed were conducted. Trials selected for analysis required a clean right and left foot strike on separate force plates, resulting in a range from 1 to 6 usable trials for each participant at each speed. Kinetics were introduced by applying ground reaction forces and twisting moment acting at the foot center of pressure and calculating ankle, knee, and hip torque based on standard inverse dynamic approach. Power of the shank and thigh (and knee joint) was then computed from the knee joint torque and segment angular velocities. Angular velocities and accelerations were computed with a 5-point Lagrange equation. All raw kinematic and kinetic signals were filtered at 10 Hz with a fourth-order zero-lag Butterworth filter prior to model processing. Although 3D joint kinetics were calculated, only knee kinetic data in the sagittal plane are discussed in this paper.

Each trial required a clean force plate heel strike and toe off of left and right feet (on separate plates) and at least a full cycle (peak knee flexions) of kinematic data for both sides. Data were cycled for left and right sides (0–100% cycle) of each walking trial using a Fourier series. Gait speed was computed by dividing the stride distance by stride time (anterior-posterior pelvis origin displacement and time from heel strike to heel strike). So that results could be presented in terms of phases of the gait cycle, common divisions were used on the basis of the recommendations of Kirtley (35) in Table 1.

Experimetal Design

Development and testing of the encoding scheme was executed in two sequential studies. The first study develops the method of encoding and presents results of applying this encoding to multiple gait trials at normal and fast walking speeds. The second study develops the method for predicting encoding sequence during movement and presents results of applying this prediction to the gait trials above.

STUDY 1: ENCODING JOINT DYNAMICS BY ENERGY STATE

Proposed Encoding Scheme

The proposed methodology is based on a classical mechanical model of energy transference between connected bodies in a kinetic chain (5). The model is attractive for the present application because it discretizes the combination of torque and

Table 1. *Gait cycle divisions used in the analysis of mode prediction accuracy*

Symbol	Description
FDS	First double support (ipsilateral heel strike to contralateral toe off);
MST	Mid-stance or initial single support (contralateral toe off to ipsilateral minimum vertical ground reaction force);
TST	Terminal-stance or final single support (ipsilateral miniumum vertical ground force to contralateral heel strike);
SDS	Second double support (contralateral heel strike to ipsilateral toe off);
ISW	Initial swing phase (ipsilateral toe off to ipsilateral maximum knee flexion angle);
MSW	Mid-swing phase (ipsilateral maximum knee flexion angle to ipsilateral knee angle inflection);
TSW	Terminal swing phase (ipsilateral knee angle inflection to ipsilateral second heel strike).

angular velocity waveforms of a joint into a sequence of energy transfer or "power flow" modes. The power flow modes identify the conditions that dictate when the joint is losing or gaining energy and to what extent energy is generated or dissipated by the muscles (or joint motor) based on torque and/or velocity switches (zero crossings) that occur during cyclic gait motion.

Sequence of Power Flow Modes

Consider two connected bodies with net torque τ acting about the joint such that $\tau = \tau_p = -\tau_d$(assuming Newtonian joint) and with the two bodies rotating at speeds of ω_d and ω_p, where subscript d represents the distal (shank) segment and p represents the proximal (thigh) segment. The power available at the joint for the distal segment is $P_d = \omega_d * \tau_d$ and at the corresponding joint of proximal segment is $P_p = \omega_p * \tau_p$. Summing these two powers (being coincident points and scalars), we arrive at the net joint power, P_j

$$P_j = P_d + P_p = \tau_p * (\omega_p - \omega_d) = \tau * \omega \qquad (1)$$

where ω is the relative angular velocity of the joint. As illustrated in Fig. 2, the mode of power flow is determined from signs of P_d and P_p, as well as the sign of the resulting net power, P_j:

$$\begin{aligned}
&\text{if } P_p < 0 \text{ and } P_d < 0 \text{ and } P_j < 0 \text{ then } Mode = \text{A}\\
&\text{if } P_p < 0 \text{ and } P_d > 0 \text{ and } P_j < 0 \text{ then } Mode = \text{B}\\
&\text{if } P_p < 0 \text{ and } P_d > 0 \text{ and } P_j > 0 \text{ then } Mode = \text{C}\\
&\text{if } P_p < 0 \text{ and } P_d > 0 \text{ and } P_j > 0 \text{ then } Mode = \text{D}\\
&\text{if } P_p < 0 \text{ and } P_d < 0 \text{ and } P_j > 0 \text{ then } Mode = \text{E}\\
&\text{if } P_p < 0 \text{ and } P_d < 0 \text{ and } P_j < 0 \text{ then } Mode = \text{F}
\end{aligned} \qquad (2)$$

Equation 2 shows that the sign of the net joint power is dependent on the sign of the knee joint torque, τ; the sign of the distal and proximal segment angular velocities, ω_p and ω_d; and the sign of the relative angular velocity of the knee, ω. Because the methodology uses net joint torques, it does not distinguish between uniarticular and biarticular muscle contributions. Therefore, the term "knee muscles" used below to describe the different modes of energy transfer refers specifically to the net joint moment contribution of muscles crossing the knee and other joints.

Mode A (Fig. 2, *top center*) represents the condition in which energy of both thigh and shank is decreasing and therefore the knee muscles must dissipate all the energy. Mode B (Fig. 2, *top right*) represents the condition in which energy is transferring distally; decreasing for the thigh and increasing for the shank. Here the thigh is losing more energy than is gained by the shank, which means the knee muscles must dissipate this excess energy. Mode C (Fig. 2, *bottom right*) also represents the condition in which energy is transferring distally; as with mode B, decreasing for the thigh and increasing for the shank. But here the thigh is losing less energy than is gained by the shank, which means the knee muscles must generate this excess energy. Mode D (Fig. 2, *bottom center*) is similar to mode A, except that energy is now increasing for both thigh and shank at the knee, requiring knee muscles to do all the work. Mode E (Fig. 2, *bottom left*) is the condition in which energy is transferred proximally; shank energy is decreasing and thigh energy is increasing. Here the increase in thigh energy is more than the energy loss of the shank, requiring knee muscles to generate the excess energy. Mode F (Fig. 2, *top left*) is also the condition in which energy is transferred proximally; as with mode E, shank energy is decreasing and thigh energy is increasing. But here the increase in thigh energy is less than the energy loss of the shank, requiring knee muscles to dissipate the excess energy.

Modes A and D are therefore "no transfer" modes in which the knee does all the work in dissipating (mode A) or generating (mode D) segmental energy. Modes B, C, E, and F are "transfer modes" and represent conditions in which energy is transferred between segments distally (modes B and C) or proximally (modes E and F). For transfer modes, the knee regulates segmental energy by either generating (modes C and E) or dissipating (modes B and F) the energy imbalance at the joint.

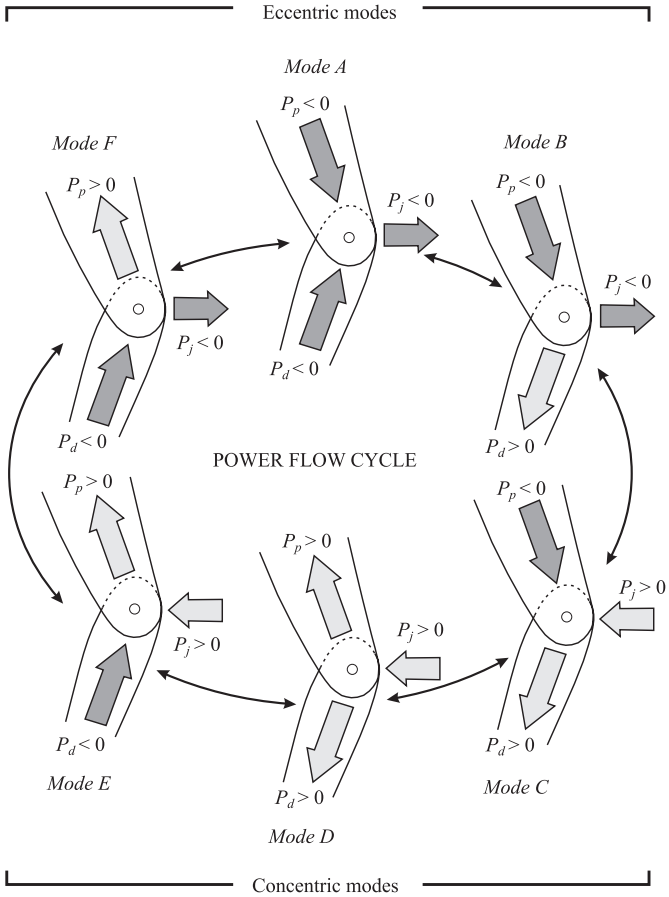

Fig. 2. Illustration depicting the power flow cycle of the knee and its dependence on both absolute segment powers and relative joint power. Arrows along the segments indicate whether the distal and proximal segment energy at the knee is increasing (open) or decreasing (shaded). Arrows at the joint indicate how the knee muscles contribute to energy transfer between segments, by either adding energy (open) or dissipating energy (shaded). The result is 6 different "modes" of power flow: 3 modes that represent power dissipation (eccentric muscle net power) and 3 that represent power generation (concentric muscle net power). Each transition mode in the cycle is triggered by a change in sign of 1 of 3 powers [distal segment, proximal segment, or relative (net) power] and thus follows a logical order.

Results

Mode sequence during normal and fast gait. As previously described, lower extremity gait data were acquired for eight adult females at preferred and fast walking speeds. This resulted in 33 walking trials for preferred speed gait and 25 walking trials for fast speed gait. Preferred walking speed was 1.17 ± 0.16 m/s, and fast walking speed was 1.55 ± 0.21 m/s. Paired *t*-tests between preferred and fast speeds for the eight subjects were significant ($P < 0.001$). Each trial required a clean force plate heel strike and toe off of left and right feet (on separate plates) and at least a full cycle of kinematic data for both sides (typically 2 cycles are captured). By using left and right sides, a total of 66 preferred speed trials and 50 fast speed trials was analyzed.

Joint kinematics and kinetics were computed for each knee, cycled from 0 to 100% cycle, and averaged. Kinematic and kinetic data for the knee joint in the sagittal plane during preferred speed and fast walking are shown in Fig. 3 (left and right respectively). The shaded band represents ±1 standard deviation. The *top* plots show the angular velocities of the shank (ω_d, shown in violet) and thigh (ω_p, shown in green), the middle plots show knee joint relative velocity (ω, shown in red), and the bottom plots show knee joint torque (τ, shown in blue). Gait cycle divisions described previously are also shown below the graphs and are represented by dotted vertical lines in each plot.

Also shown are color-coded vertical lines representing each switch or zero crossing that occurs in each signal during the gait cycle. These switches are the biomechanical events that trigger each power mode transition and are represented as follows. Knee torque switches ($\tau\Delta$) are indicated by vertical blue lines; knee angular velocity switches ($\omega\Delta$) are indicated by the vertical red lines, and thigh and shank angular velocity switches ($\omega p\Delta$ and $\omega d\Delta$) are shown by the vertical violet and green lines, respectively.

Difference between data at the two different walking speeds is clearly the higher variability at higher walking speeds, which is more pronounced for joint torques than for joint velocity. Note that although segment angular velocities increase, these increases are modest compared with torque amplitude increase. This explains the difference between power curve amplitudes for the two gait speeds in Fig. 4.

Figure 4 represents the net joint power (*top* plots) and the resulting power mode sequence (*bottom* stair plots). Superimposed on these plots are the mode switch lines (with switch labels, shown in Fig. 3) that dictate the mode sequence. Also shown are the divisions of the gait cycle. It is interesting to note that some mode transitions occur in close proximity to the traditional gait cycle divisions.

These data show the sequence of power flow modes is essentially the same for both normal and fast walking speeds, suggesting that sequence control is independent of walking speed (within the limits studied here). The sequence of energy transfers that allows the knee to facilitate gait between preferred to fast walking speeds is therefore:

?F E B C F A B C F A?

The initial and final mode letters are labeled "?" to indicate that the mode at heel strike is somewhat uncertain, as several switches occur in close proximity.

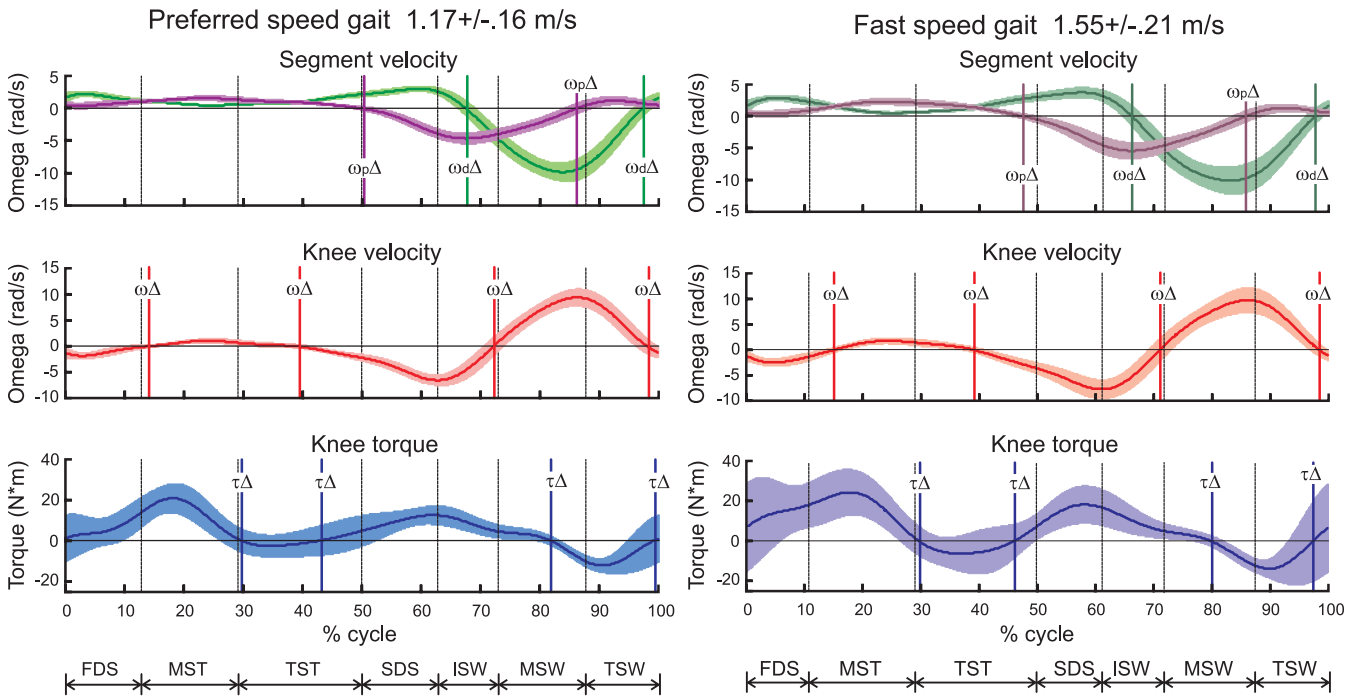

Fig. 3. Knee joint kinematics and kinetics during preferred speed (*left*) and fast speed (*right*) gait. In the *top* plots, angular velocity of the thigh (ω_p) is shown in violet, and angular velocity of the shank (ω_d) is shown in green. In the *middle* plots, relative velocity of the knee (ω) is shown in red. In the *bottom* plots, knee torque (τ) is shown in blue (extensor torque is positive). The shaded bands about the mean curves represent ±1 standard deviation from the sample mean. Mode switches are shown for each signal with vertical solid lines and switch indicator (Δ).Vertical dotted lines represent the traditional divisions of the gait cycle and correspond to labels shown at the bottom of the plot.

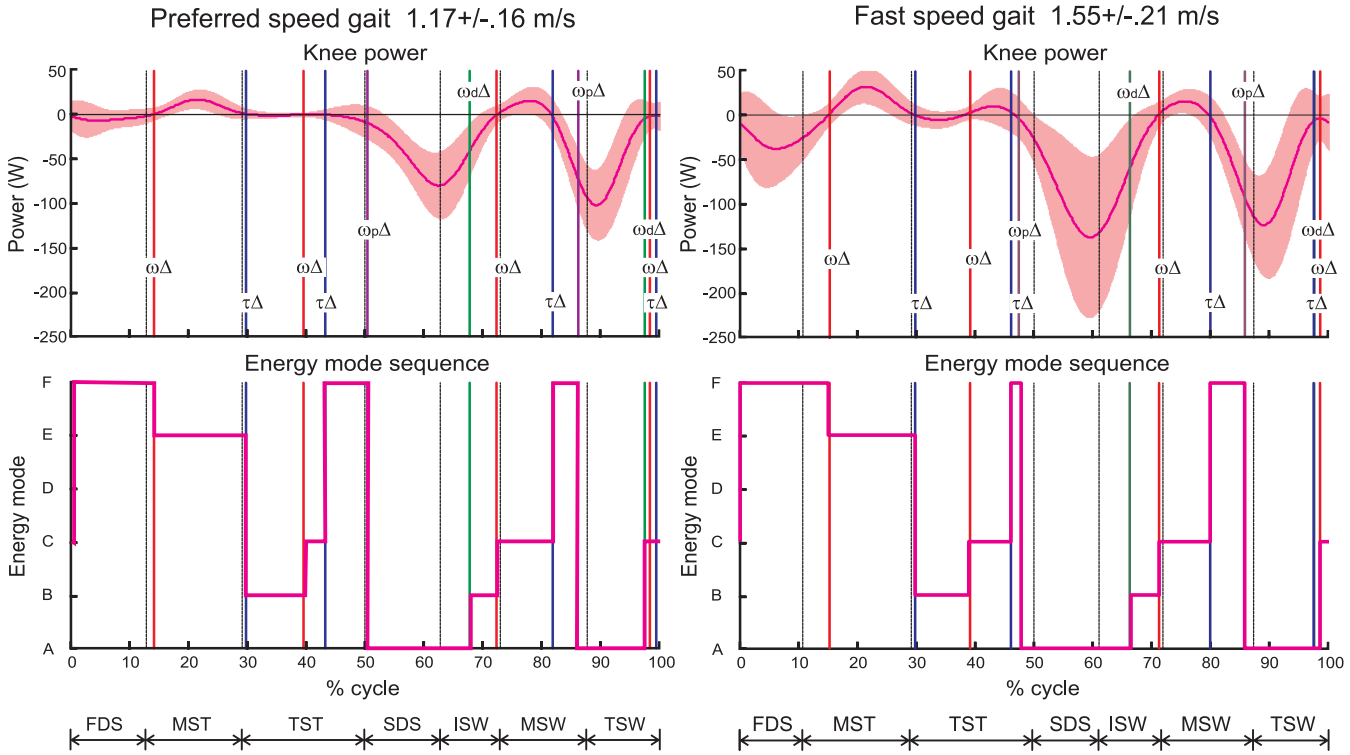

Fig. 4. Knee power and power mode sequence during preferred speed (*left*) and fast speed (*right*) gait. In the *top* plots, joint power is shown in magenta (negative is dissipative). The shaded bands about the mean curves represent ±1 standard deviation from the sample mean. Mode switches are shown for each signal with vertical solid lines and switch indicator (D). Vertical dotted lines represent the traditional divisions of the gait cycle and correspond to labels shown at the bottom of the plot.

To make sense of the sequence, first consider the meaning of couples of adjacent modes. Couples F→E and B→C represent relative velocity switches (ωΔ). Couples F→A and A→B represent switches in absolute velocity of the thigh (ωpΔ) and shank (ωdΔ) segments, respectively. Finally, the E→B and C→F couples represent torque switches (τΔ). More important, however, is the sequence in which these energy transitions occur. For example, the segment

$$F \rightarrow E \rightarrow B \rightarrow C$$

occurred in the first half of the gait cycle and was present in 62% of trials for both preferred speed and fast speed gait. The segment

$$A \rightarrow B \rightarrow C \rightarrow F$$

occurred in the last half of the gait cycle and was present in 76% of preferred speed trials and 86% of fast speed trials. Most striking, however, was the segment

$$B \rightarrow C \rightarrow F \rightarrow A$$

which occurred in more than 90% of trials at both gait speeds. It can be seen in Fig. 4 (*bottom* plot) that this segment occurs twice.

This latter observation is interesting in the context of knee dynamics during gait. In Fig. 4 (*bottom*), this repeating segment can be seen starting at ~30% cycle and again at ~65% cycle. Noting the knee torque and velocity curves in Fig. 3 and the knee power curve in Fig. 4 (*top*), it can be seen that between 30 and 100% cycle, switches in torque and velocity are coordinated such that they produce a repeating power curve. Indeed, the same sequence of switches occur (ωΔ→τΔ→ωpΔ→ωdΔ). It is worth noting that the polarity of switches is different for each repeating sequence, but as such, they result in the same power signature.

As suggested by the joint power plot in Fig. 4, the role of the knee during gait is mostly to dissipate segment energy. Energy dissipation was substantially required during second double support/initial swing and during terminal swing phase, but also required (to a lesser extend) after heel strike and in late mid-stance phase. Although less in amplitude, power generation was observed mostly during early mid-stance and mid-swing phase. Terminal stance phase power was lowest for both gait speeds, but generation and absorption were more pronounced for faster walking than for preferred speed walking where powers were nil.

STUDY 2: PREDICTION OF ENCODING SEQUENCE FROM SIMULATED SENSOR DATA

Implications for TFP Control

The previously mentioned findings suggest that prosthetic knee control during gait could be achieved by maintaining this cyclic mechanical energy transfer pattern across the knee joint. Because the encoding method is activity independent, the concept could also be applied to other joints and locomotor activities where feedforward control is advantageous. This section discusses the unique properties of mode switch behavior that make such a robust control

requirement possible. Again, focus is on controlling an artificial knee during gait.

As noted in Figs. 3 and 4, each mode transition in the cycle is triggered by a change in sign (zero cross-over) of one or more of these four variables, referred to as "Δswitches." Figure 5 shows that the current mode (open circles) can switch to other modes (light gray shaded circles) when specific variable(s) change sign, identified by labels on the arrows extending from the current mode. The label $\tau\Delta$, for example, indicates a torque switch (zero crossing). Modes represented by shaded circles require only one variable switch to occur. Modes represented by dark gray shaded circles require two variables to switch simultaneously.

Thus by monitoring switch times of three metrics (that can potentially be measured with an artificial knee device): τ = knee torque; ω = knee flexion velocity; and ω_d = shank angular velocity (and the metric ω_p = thigh angular velocity, computed from $\omega+\omega_d$), the kinetics of the knee can be reduced to a sequence of power flow modes that describe how the joint is regulating energy generation and dissipation during a movement activity or task. More importantly, because any future mode is dependent on certain specific switches occurring (as illustrated in Fig. 5), monitoring the above signals can also be used to predict the next mode that will occur.

Mode Prediction

Mode prediction can be accomplished by determining the probability that, at any given point in time, one or more of the above metrics will change sign in the near future.

For the sake of simplicity, we can model this probability as $p = z(y,0,s)$ where z is a normal distribution function, y is the metric in question, and s is a measure of the signal's standard deviation. The 0 term simply indicates we are interested in knowing where y is with respect to its zero, regardless of the signal's mean. To estimate s we can compute the metric's standard error over a sufficiently long epoch (i.e., in this case, an entire gait cycle) using $s = \sigma_Y/\sqrt{N}$ where N is the length of the record and σ_Y is the standard deviation of Y. To improve our prediction, we can also make use of signal time derivatives to give an indication of which direction the signal is moving when near the zero crossing.

Now let us assume we have a knee prosthesis that provides signals representing estimations of the four metrics above, their time derivatives, plus an estimate of the standard error for each of the four metrics.

$$\{\tau, \dot{\tau}, s_T\}; \{\omega_p, \dot{\omega}_p, s_P\}; \{\omega_d, \dot{\omega}_d, s_D\}; \{\omega, \dot{\omega}, s_J\} \quad (3)$$

Also let us assume we are sampling from the prosthesis over intervals of C, where C = portion of the gait cycle. We desire to predict the next mode that will occur in the interval that follows C. Finally, we can specify a threshold probability α for detecting an impending zero crossing of any of the four metrics. In this study a $\alpha = 0.05$ threshold was used, which can be interpreted as the 95% confidence level at which a change in sign of a given metric will occur within the interval C.

The first step is identifying the current mode from the sampled signal. As described above we can find the modes by examining the signs of each metric. To simplify, we can first compute the powers segment and joint powers and then apply a logical test, as shown above in *Equation block 2*. This results in a mode (*Md*) value for each sample point.

Forward prediction requires computing the probability that any one or more metric is to change sign, as described above.

$$p_T = \mathbf{z}(\tau_J, 0, s_T);\ p_p = \mathbf{z}(\omega_P, 0, s_P);\ p_D = \mathbf{z}(\omega_D, 0, s_D);\ p_J = \mathbf{z}(\omega_J, 0, s_J); \quad (4)$$

If a signal has already crossed the zero line but is still within the detection threshold, we can reduce the probability to zero to avoid such erroneous detections simply multiplying the signal by its time derivative and testing the sign - if negative then the signal is approaching the zero. If positive, then the signal has already crossed. For example, if $\tau * \dot{\tau} > 0$ then $p_T = 0$.

By using the schematic illustrated in Fig. 5, the logical test set for predicting the next mode (*nxMd*) follows as such, using current mode A as an example:

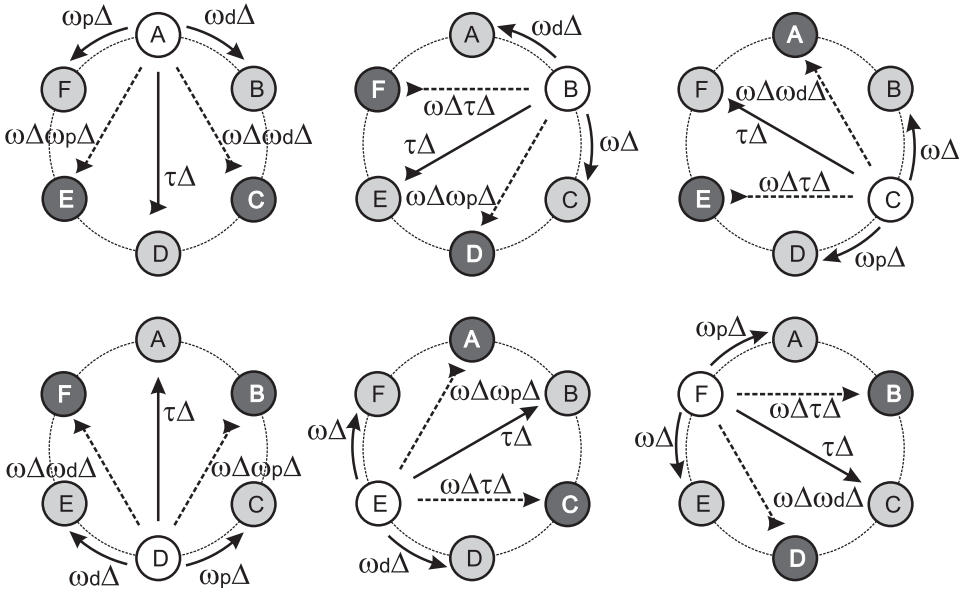

Fig. 5. Mode switch behavior. For a current mode (open circles), the next possible modes are indicated with gray filled circles. The arrow labels indicate the quantity(ies) that must change sign for that mode to occur next. The dark shaded circles represent modes than cannot be switched to unless two quantities change sign simultaneously. The light shaded circles require a change in sign of only one variable.

$$
\begin{aligned}
&\text{if current } Md = \text{A and...}\\
&\text{if } p_P > \alpha \quad \text{then } nxMd = \text{F}\\
&\text{if } p_D > \alpha \quad \text{then } nxMd = \text{B}\\
&\text{if } p_T > \alpha \quad \text{then } nxMd = \text{D}\\
&\text{if } p_D * p_J > \alpha \quad \text{then } nxMd = \text{C}\\
&\text{if } p_P * p_J > \alpha \quad \text{then } nxMd = \text{E}\\
&\text{else } nxMd = \text{A}
\end{aligned}
\tag{5}
$$

The logical tests follow similarly for the other modes. If more than one potential mode crossing is probable, the mode switch with the highest probability is selected.

To test this concept, sensor data for the walking trials above were input to the mode identification and prediction algorithm. The signals consisted of joint torque and segment angular velocities and relative joint velocity. For each walking trial (one full gait cycle), samples were randomly drawn (k = 500 samples) at frame lengths of C = 2% gait cycle (20 frames) and the signals averaged over the interval. Signals were then combined to compute the three power terms in *Eq. 1* and the *logical test 2* was then applied to identify the current mode. The identified current mode was then compared with the actual current mode and scored as 1 if the mode was correct and 0 if incorrect. Identification accuracy was computed by averaging the binary scores over the k random samples.

Then, the next mode was predicted by entering the signal time derivatives (also averaged over the interval) and a measure of standard error, and applying the *logical test 5*. Two forward search lengths were tested: C = 2% cycle and C = 4% cycle. The predicted next mode was then compared with the actual next mode and scored as above. Current and next mode prediction accuracies were then sorted into seven bins according to where the mid-point of the random interval fell within the seven prescribed phases of the gait cycle. These data were then averaged across the set of walking trials to give average prediction accuracy for current mode and next mode for each phase of the gait cycle. These results are shown with bar charts in Fig. 6.

Dynamic Encoding Prediction

The data show that the ability to identify the current power mode is very high for both C = 2% and C = 4% search lengths (only the 2% result is shown in Fig. 6 for current mode). The

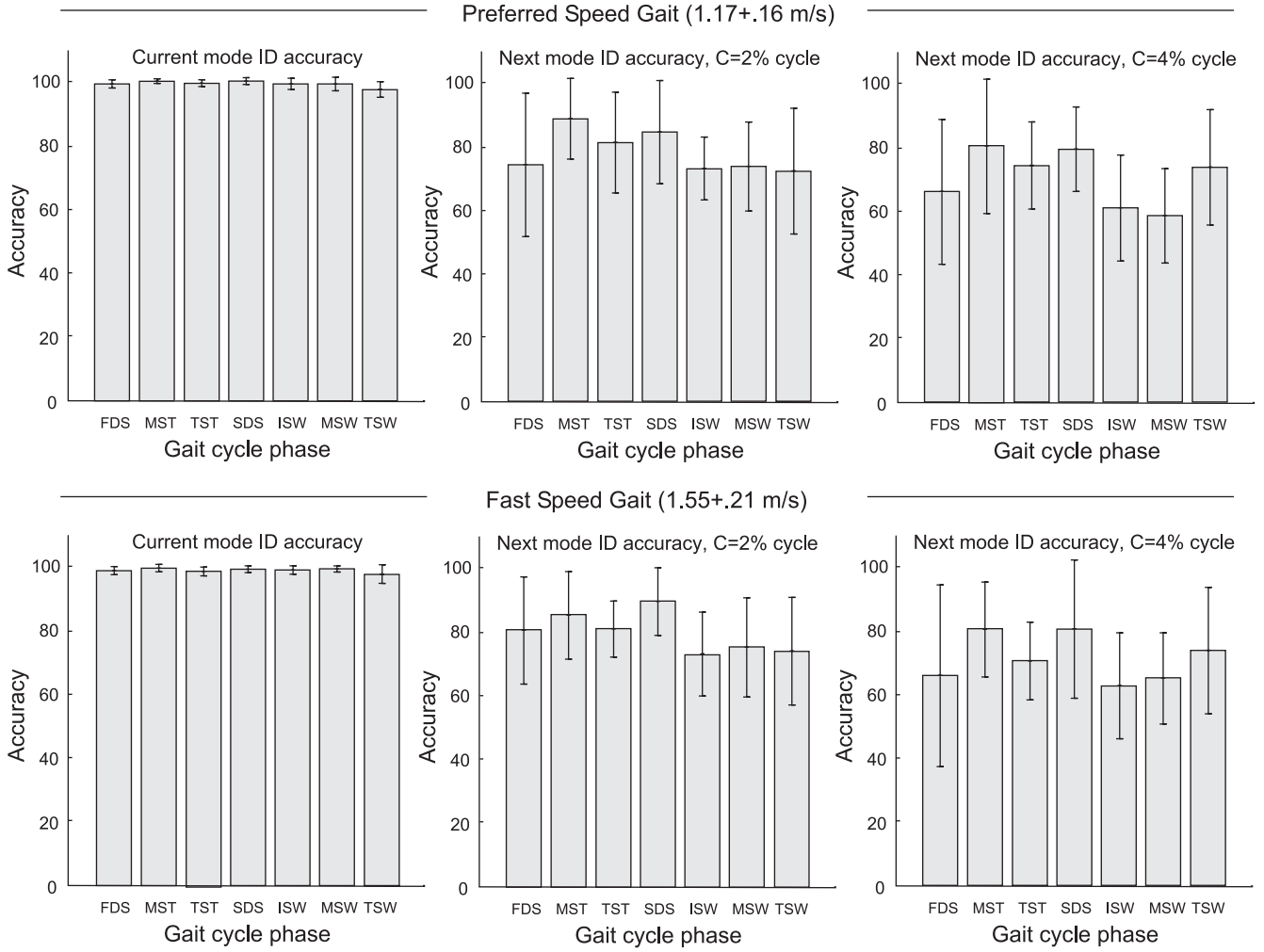

Fig. 6. Prediction accuracy of current and next modes for the seven phases of the gait cycle, at preferred speed (*top* plots) and fast speed (*bottom* plots) gait. Current mode identification accuracy is shown in the *left* column. Next mode identification accuracy with a search length of 2% cycle, and 4% cycle, are shown in the *middle* and *right* columns, respectively. Results were binned according to gait cycle phase. Error bars represent ±1 SD from the bin mean.

interval length of 2% cycle is therefore sufficient to detect the current mode. When employing the next mode detection algorithm, the next mode accuracy was higher for C = 2% than C = 4% cycle and was slightly better for fast speed walking compared with preferred speed walking. At C = 2%, prediction accuracy for fast walking was above 80% for all phases of the gait cycle and above 75% for preferred speed walking. At C = 4%, prediction accuracies in some phases of the gait cycle fell below 60%.

Portions of the gait cycle with the highest prediction accuracy were mid-stance or initial single support and second double support phases. Lowest accuracy was observed during first double support of stance phase and initial swing phase and mid-swing phase of swing phase, especially when search length is extended to 4% cycle.

DISCUSSION

The motivation for this research is to enhance the capacity of TFP control by making use of the artificial limb sensory potential and biomechanical behavior of single degree-of-freedom joints to derive a simple encoding sequence that describes the current and future energy requirements of the joint. Although there is still great controversy regarding CNS encoding of intact human joint movements, the underlying premise of this research is that such encoding is likely related to the kinematics and kinetics of the joint (9, 16). Development of neural interfaces for neuroprostheses might benefit from using control architectures that better represent the biomechanical function of the replaced joint (17, 24).

Results of *study 1* show that joint kinetic magnitude and time history agree with data published by others (19, 58). Furthermore, results show it is possible to encode the dynamics of the knee joint by its sequence of energy transfer states and that this sequence appears to have smaller subsequences that define the energy state required to stabilize the joint (i.e., heel strike to terminal single support) and to dissipate energy of the joint (i.e., second double support and swing phase). The sequence was preserved at both normal and fast walking speeds.

Results of *study 2* exploited the fact that the underlying biomechanical switching events that define the different energy states are simple sense (sign) changes in the input sensor signals. Because the switching behavior is finite, a probabilistic model was used to predict which energy state is most likely to occur next given the joint's current energy state. Simulations found that the current energy state identification accuracy was very high (~99%) and that >80% and >60% accuracy in next mode prediction was possible when searching ahead 2% and 4% of the gait cycle, respectively.

These data suggest that the future energy state of the knee can be predicted in advance of switch events, provided there are sensor data to monitor the joint's energy state, such as with an artificial limb. Furthermore, because this paper uses able-bodied motion analysis data to derive a model to provide the knee joint sensor signals, the concepts put forth here may also be of some value in animal motor control research and for applications in functional electrical stimulation and neuroprosthetics.

The encoding method can be used for any human activity in which any two adjacent segments have relative motion (whether externals forces are present or not), such as upper extremity reaching tasks or during common activities of daily living such as sit-to-stand, gait initiation and termination, or sport and leisure activities such as running or jumping. Additional studies are required for capturing data for these different activities and more importantly their transitions for able-bodied persons and transfemoral amputees.

Interpreting the Energy Mode Sequence of the Knee

A summary of the sequence of biomechanical switch events during gait is shown in Fig. 7. The emerging pattern suggests joint stabilization dominates in the pre- and early-stance phase of gait, followed by two identical sequences of energy dissipation: one in the terminal stance/early swing phase and the other in the mid-swing/terminal swing phase.

The stabilization sequence, which commences prior to heel strike, enables the knee to accept load bearing following heel strike until end of mid-stance phase. Prior to heel strike the knee has energy mode A (85–98% cycle), which means both shank and thigh are decelerating and the knee muscles are absorbing the excess energy. The short event of heel strikes appears to indicate mode C is most common, and according to Fig. 2, this would be the result of a concentric knee contraction to give more energy to the shank for stabilizing heel strike. The next mode quickly becomes F (~2% to 13% cycle for preferred speed gait and ~0–15% cycle for fast gait) in which the energy of the shank is transferred to the thigh but regulated by knee muscle dissipation. This is followed mode E, which requires knee energy input to increase thigh energy (and upper body energy) during single support as the shank energy is diminished. This mode terminates when a torque switch from extensor to flexor occurs at ~30% cycle.

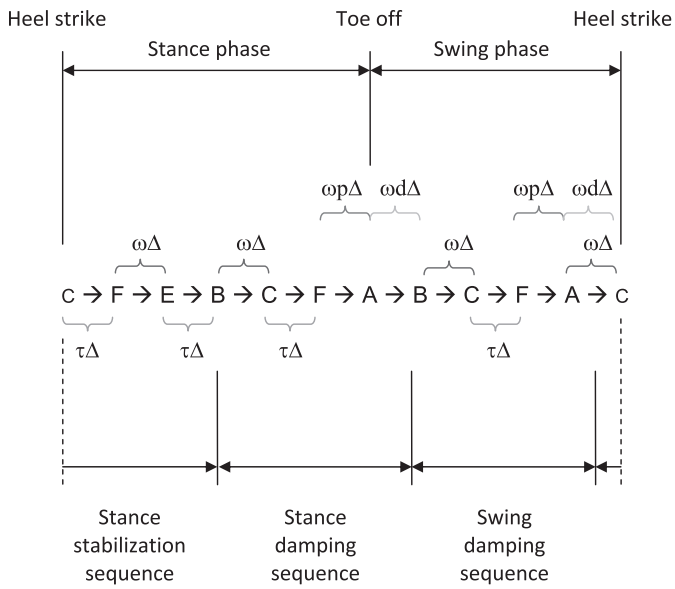

Fig. 7. Schematic showing the biomechanical mode switching sequence for the knee during walking gait and its temporal relationship with the major phases of the gait cycle and the energy demand sequence of the knee. Note the latter is offset from the standard gait cycle, involving a stabilization sequence that precedes heel strike and lasts until mid-stance followed by two damping sequences, which dissipate energy of the folding limb during second terminal stance and double support phases and of the extending limb during mid-to-terminal swing phase.

Two successive sequences of B→C→F→A then follow to complete the gait cycle, controlling energy dissipation of the folding knee joint in terminal-stance phase through second double support phase (stance phase dissipation sequence) and the extension of the knee joint through mid-swing and terminal swing (swing phase dissipation sequence); in both cases shank energy dissipation is required following a rapid energy gain.

During the stance portion of this sequence the tibia accelerates as the body center of mass passes over the stance foot while the thigh is decelerating and requiring the knee to absorb energy (mode B). The transition to mode C follows a reversal in the knee flexion angle when tibia rotation velocity exceeds the thigh rotation velocity (knee flexion minima); the knee reverses direction to allow the tibia to accelerate while the thigh is decelerating, requiring a small amount of knee muscle energy generation (more pronounced in fast speed gait than preferred speed gait). Knee torque switches from flexor to extensor at ~45% cycle, switching the mode to F. Here the energy of the thigh increases briefly to balance the knee joint's inability to absorb all the energy from the shank. The thigh reverses rotation direction at ~50% cycle, switching to mode A, in which both shank and thigh require energy dissipation from the knee as the ankle performs its plantar flexor power burst to enable swing phase of the limb.

This is followed by the swing damping sequence, which has the same energy signature as the stance damping sequence. After the leg is released from the ground, the tibia rotation switches rotation direction and accelerates using energy from the thigh while the knee absorbs the excess energy (mode B). The knee reaches maximum flexion angle and switches direction at ~70% cycle, which switches the mode to C. With this mode the knee generates a small amount of energy to assist the shank in toe clearance. The torque switch at ~80% cycle from extensor to flexor causes a switch to mode F in which the thigh energy increases briefly as shank energy is being absorbed by the knee. This is followed by mode A (~88% cycle) in which knee is required to absorb energy of the thigh and shank to decelerate the leg prior to heel strike.

Figure 3 shows the reason this sequence is repeated. Because both velocities and torques have reversed polarity for each of the two dissipative phases and the velocity and torque switches occur in the same order, the energy signature is the same. Controlling the energy dissipation during both terminal stance and swing phase is essentially the same, with the exception that torque dominates the energy demands during stance and velocity dominates the energy demands during swing; Fig. 4 shows these dissipative energy sequences are similar in terms of energy generation and absorption.

It is also noteworthy that mode D does not appear in the sequence of energy modes experienced by knee during walking when averaged across the sample. Mode D (the opposite of mode A, which occurs frequently in gait) is a condition where the proximal and distal muscles do all the work in generating knee power. According to the sequence of joint energy states, the knee is rarely generating all the energy required to accomplish steady-state gait and is mostly stabilizing motion by controlling energy dissipation (mode A) or aiding in energy transfer by regulating dissipation (modes B and F) or generation (modes C and E) of energy.

A recent study by Dumas and Cheze (14) and further extensions of this work (52) appear to support the explanation for why mode D is absent in normal gait. These studies used the 3D angle between joint torque and velocity vectors to determine when the joint would be in a "driving" or "stabilizing" mode. Findings showed that the knee acts more to stabilize than to drive motion during normal gait. This agrees with the findings of the present study and may also explain why current state-of-the-art TFPs (mechanical or microcomputer passive controlled) have worked so well for enabling gait for transfemoral amputees. However, gait is but only one of many common activity of daily living associated with full mobility. For example, mode D would be crucial for rising from a chair or climbing a step in which the knee must provide a driving torque to enable task completion.

Limitations of Interpretation

Although the term "switch" is used here to indicate the zero crossing of the biomechanical signal, for knee angular velocity it also represents the maxima and minima of the knee flexion angle curve. These events are relatively stable for steady-state walking and represent the typical knee angle sequence of load acceptance maxima, mid-stance minima, swing phase maxima (peak), and terminal swing minima (just prior to heel strike). Even people with pathological gait whose knee curves and may have different magnitudes and relative peak timing typically exhibit a knee angle pattern with the same sequence of maxima and minima. In some cases the terminal swing minima could occur after registration of heel strike. This explains the difficulty in designating a mode sequence at heel strike.

Not only do switches in relative knee velocity affect the power flow mode, but so do switches in absolute angular velocity of the shank and thigh. These switches also occur in a typical fashion during gait; the thigh and shank both rotate forward for most of stance phase, with the thigh reversing direction to allow for heel rise at ~50% cycle and reversing again at terminal stance phase. The shank reverses direction shortly after toe-off (~66%) and reverses again just prior to second heel strike. This latter switch often occurs simultaneous with knee relative angle switch. Variance in timing of this switch could also impact the starting and/or ending symbols of the mode sequence.

Torque switches are less consistent than velocity switches, due in part to the greater uncertainly in knee torque calculations compared with velocity calculations (as indicated by the wider bands in the torque plot compared with angular velocity plots). This simply means that torque switch times may be quite variable across (and even within) individuals. Because kinetic data are often collected at higher sampling frequencies than kinematic data and gait cycle events are defined by force plate events (bilateral heel strike and toe off), small discrepancies can occur in kinematic cycling that could also affect the switch timing of knee torque. However, by analyzing numerous trials (66 for preferred-speed gait and 50 for fast-speed gait) the consensus agreement on the sequence of energy modes was high, exceeding 75%, suggesting that appropriate care was taken in synchronizing kinematic and kinetic data sets. Furthermore, identification of current energy mode and next energy mode in simulations was high (typically >80%) and did not appear to be appreciably affected by uncertainty in torque switches. However, these and other effects are yet to be tested.

Conclusions

This paper presents and tests a framework for *1*) encoding joint dynamics into energy states using kinematic and kinetic joint sensor data and *2*) using the encoding sequence properties (based on classical mechanical principles) to predict the future energy state of the joint, without a priori knowledge of the activity sequence. The intended application is for enhancing microcontrolled prosthetics by making use of the embedded sensory potential of artificial limbs, and classical biomechanical principles of joint articulation and actuation, to facilitate development of control architectures that reflect how neural control of natural joint motion may be controlled.

When applied to the knee during preferred and fast speed walking in 8 human subjects (66 preferred-speed trials and 50 fast-speed trials), it was found that joint energy states could be consistently sequenced (75% consensus) according to mechanical energy transference conditions, and subsequences appeared to reflect the stability and energy dissipation requirements of the knee during gait.

When biomechanical constraints are applied to the energy transfer conditions, simulations indicated that, when given various statistical parameters of the sensor readings, it was possible to predict the future energy state with an accuracy of >80% when 2% cycle in advance (~20 ms) of the switch and >60% for 4% or ~40 ms advance. Current device sampling rates can provide better than 200 ms updating and, therefore, should be sufficient to accommodate controller response to such predictions.

Additional research is required to explore whether this encoding algorithm can be used to identify submodes of other human activity that are relevant to TFP control, such as chair and stair activities and their transitions from walking.

ACKNOWLEDGMENTS

The author acknowledges the support of former graduate student Katrina McQuoid, who was instrumental in collecting the motion analysis data used in this paper, and the financial support of the Natural Sciences and Engineering Research Council of Canada and the Canadian Institutes of Health Research Regional Partners Program.

DISCLOSURES

No conflicts of interest, financial or otherwise, are declared by the author.

AUTHOR CONTRIBUTIONS

Author contributions: C.A.M. conception and design of research; C.A.M. performed experiments; C.A.M. analyzed data; C.A.M. interpreted results of experiments; C.A.M. prepared figures; C.A.M. drafted manuscript; C.A.M. edited and revised manuscript; C.A.M. approved final version of manuscript.

REFERENCES

1. **Aleshinsky SY.** An energy "sources" and "fractions" approach to the mechanical energy expenditure problem—I. Basic concepts, description of the model, analysis of a one-link system movement. *J Biomech* 19: 287–293, 1986.
2. **Aleshinsky SY.** An energy "sources" and "fractions" approach to the mechanical energy expenditure problem—II. Movement of the multi-link chain model. *J Biomech* 19: 295–300, 1986.
3. **Aleshinsky SY.** An energy "sources" and "fractions" approach to the mechanical energy expenditure problem–III. Mechanical energy expenditure reduction during one link motion. *J Biomech* 19: 301–306, 1986.
4. **Aleshinsky SY.** An energy "sources" and "fractions" approach to the mechanical energy expenditure problem—IV. Criticism of the concept of "energy transfers within and between links". *J Biomech* 19: 307–309, 1986.
5. **Aleshinsky SY.** An energy "sources" and "fractions" approach to the mechanical energy expenditure problem—V. The mechanical energy expenditure reduction during motion of the multi-link system. *J Biomech* 19: 311–315, 1986.
6. **Asano M, Rushton P, Miller WC, Deathe BA.** Predictors of quality of life among individuals who have a lower limb amputation. *Prosthet Orthot Int* 32: 231–243, 2008.
7. **Bellmann M, Schmalz T, Blumentritt S.** Comparative biomechanical analysis of current microprocessor-controlled prosthetic knee joints. *Arch Phys Med Rehabil* 91: 644–652, 2010.
8. **Brunelli S, Averna T, Porcacchia P, Paolucci S, Di Meo F, Traballesi M.** Functional status and factors influencing the rehabilitation outcome of people affected by above-knee amputation and hemiparesis. *Arch Phys Med Rehabil* 87: 995–1000, 2006.
9. **Casabona A, Bosco G, Perciavalle V, Valle MS.** Processing of limb kinematics in the interpositus nucleus. *Cerebellum* 9: 103–110, 2010.
10. **Centomo H, Amarantini D, Martin L, Prince F.** Kinematic and kinetic analysis of a stepping-in-place task in below-knee amputee children compared with able-bodied children. *IEEE Trans Neural Syst Rehabil Eng* 15: 258–265, 2007.
11. **Davis R, Ounpuu S, Tyburski D, Gage J.** A gait analysis data collection and reduction technique. *Hum Mov Sci* 10: 575–587, 1991.
12. **Delis AL, da Rocha AF, Dos Santos I, Sene IG, Salomoni S, Borges GA.** Development of a microcontrolled bioinstrumentation system for active control of leg prostheses. *Conf Proc IEEE Eng Med Biol Soc* 2008: 2393–2396, 2008.
13. **DeVita P, Helseth J, Hortobagyi T.** Muscles do more positive than negative work in human locomotion. *J Exp Biol* 210: 3361–3373, 2007.
14. **Dumas R, Cheze L.** Hip and knee joints are more stabilized than driven during the stance phase of gait: an analysis of the 3D angle between joint moment and joint angular velocity. *Gait Posture* 28: 243–250, 2008.
15. **Durfee WK.** Control of prosthetic gait. *Curr Opin Neurobiol* 4: 920–923, 1994.
16. **Ebadzadeh M, Tondu B, Darlot C.** Computation of inverse functions in a model of cerebellar and reflex pathways allows to control a mobile mechanical segment. *Neuroscience* 133: 29–49, 2005.
17. **Eilenberg MF, Geyer H, Herr H.** Control of a powered ankle-foot prosthesis based on a neuromuscular model. *IEEE Trans Neural Syst Rehabil Eng* 18: 164–173, 2010.
18. **Elftman H.** Forces and energy changes in the leg during walking. *Am J Physiol* 125: 339–356, 1939.
19. **Eng JJ, Winter DA.** Kinetic analysis of the lower limbs during walking: what information can be gained from a three-dimensional model? *J Biomech* 28: 753–758, 1995.
20. **Fijan RS.** A three-dimensional mathematical model of the human knee joint (PhD thesis) Massachusetts Institute of Technology, 1990.
21. **Frieden RA.** The geriatric amputee. *Phys Med Rehabil Clin N Am* 16: 179–195, 2005.
22. **Ha K, Varol HA, Goldfarb M.** Volitional control of a prosthetic knee using surface electromyography. *IEEE Trans Biomed Eng* 58: 144–1451, 2011.
23. **Hafner BJ, Willingham LL, Buell NC, Allyn KJ, Smith DG.** Evaluation of function, performance, and preference as transfemoral amputees transition from mechanical to microprocessor control of the prosthetic knee. *Arch Phys Med Rehabil* 88: 207–217, 2007.
24. **Hargrove LJ, Huang H, Schultz AE, Lock BA, Lipschutz R, Kuiken TA.** Toward the development of a neural interface for lower limb prosthesis control. *Conf Proc IEEE Eng Med Biol Soc* 2009: 2111–2114, 2009.
25. **Hargrove LJ, Huang H, Schultz AE, Lock BA, Lipschutz R, Kuiken TA.** Toward the development of a neural interface for lower limb prosthesis control. *Conf Proc IEEE Eng Med Biol Soc* 2009: 2111–2114, 2009.
26. **Hargrove LJ, Li G, Englehart KB, Hudgins BS.** Principal components analysis preprocessing for improved classification accuracies in pattern-recognition-based myoelectric control. *IEEE Trans Biomed Eng* 56: 1407–1414, 2009.
27. **Hargrove LJ, Scheme EJ, Englehart KB, Hudgins BS.** Multiple binary classifications via linear discriminant analysis for improved controllability of a powered prosthesis. *IEEE Trans Neural Syst Rehabil Eng* 18: 49–57, 2010.
28. **Huang H, Kuiken TA, Lipshutz R.** A strategy for identifying locomotion modes using surface electromyography. *IEEE Trans Biomed Eng* 51: 65–73, 2009.
29. **Jiang N, Englehart KB, Parker PA.** Extracting simultaneous and proportional neural control information for multiple-DOF prostheses from the

surface electromyographic signal. *IEEE Trans Biomed Eng* 56: 1070–1080, 2009.
30. **Judge JO, Davis RB 3rd, Ounpuu S.** Step length reductions in advanced age: the role of ankle and hip kinetics. *J Gerontol A Biol Sci Med Sci* 51: M303–312, 1996.
31. **Kaufman KR, Levine JA, Brey RH, Iverson BK, McCrady SK, Padgett DJ, Joyner MJ.** Gait and balance of transfemoral amputees using passive mechanical and microprocessor-controlled prosthetic knees. *Gait Posture* 26: 489–493, 2007.
32. **Kaufman KR, Levine JA, Brey RH, McCrady SK, Padgett DJ, Joyner MJ.** Energy expenditure and activity of transfemoral amputees using mechanical and microprocessor-controlled prosthetic knees. *Arch Phys Med Rehabil* 89: 1380–1385, 2008.
33. **Kerrigan DC, Karvosky ME, Riley PO.** Spastic paretic stiff-legged gait: joint kinetics. *Am J Phys Med Rehabil* 80: 244–249, 2001.
34. **Kerrigan DC, Todd MK, Della Croce U, Lipsitz LA, Collins JJ.** Biomechanical gait alterations independent of speed in the healthy elderly: evidence for specific limiting impairments. *Arch Phys Med Rehabil* 79: 317–322, 1998.
35. **Kirtley C.** *Clinical Gait Analysis: Theory and Practice*. Philadelphia: Churchill Livingstone, 2005, p. 264.
36. **Laferrier JZ, Gailey R.** Advances in lower-limb prosthetic technology. *Phys Med Rehabil Clin N Am* 21: 87–110, 2010.
37. **Maaref K, Martinet N, Grumillier C, Ghannouchi S, Andre JM, Paysant J.** Kinematics in the terminal swing phase of unilateral transfemoral amputees: microprocessor-controlled versus swing-phase control prosthetic knees. *Arch Phys Med Rehabil* 91: 919–925, 2010.
38. **McGibbon CA, Krebs DE.** Discriminating age and disability effects in locomotion: neuromuscular adaptations in musculoskeletal pathology. *J Appl Physiol* 96: 149–160, 2004.
39. **McGibbon CA, Krebs DE.** Compensatory gait mechanics in patients with unilateral knee arthritis. *J Rheumatol* 29: 2410–2419, 2002.
40. **McGibbon CA, Krebs DE, Puniello MS.** Mechanical energy analysis identifies compensatory strategies in disabled elders' gait. *J Biomech* 34: 481–490, 2001.
41. **McGibbon CA, Krebs DE, Scarborough DM.** Rehabilitation effects on compensatory gait mechanics in people with arthritis and strength impairment. *Arthritis Rheum* 49: 248–254, 2003.
42. **McGibbon CA, Puniello MS, Krebs DE.** Mechanical energy transfer during gait in relation to strength impairment and pathology in elderly women. *Clin Biomech (Bristol)* 16: 324–333, 2001.
43. **McGill SM, Dainty DA.** Computer analysis of energy transfers in children walking with crutches. *Arch Phys Med Rehabil* 65: 115–120, 1984.
44. **Miller WC, Deathe AB.** A prospective study examining balance confidence among individuals with lower limb amputation. *Disabil Rehabil* 14–15: 875–881, 2004.
45. **Morgenroth DC, Orendurff MS, Shakir A, Segal A, Shofer J, Czerniecki JM.** The relationship between lumbar spine kinematics during gait and low-back pain in transfemoral amputees. *Am J Phys Med Rehabil* 89: 635–643, 2010.
46. **Nielsen JL, Holmgaard S, Jiang N, Englehart K, Farina D, Parker P.** Enhanced EMG signal processing for simultaneous and proportional myoelectric control. *Conf Proc IEEE Eng Med Biol Soc* 2009: 4335–4338, 2009.
47. **Olney SJ, MacPhail HE, Hedden DM, Boyce WF.** Work and power in hemiplegic cerebral palsy gait. *Phys Ther* 70: 431–438, 1990.
48. **Orendurff MS, Segal AD, Klute GK, McDowell ML, Pecoraro JA, Czerniecki JM.** Gait efficiency using the C-Leg. *J Rehabil Res Dev* 43: 239–246, 2006.
49. **Phillips CA.** Sensory feedback control of upper- and lower-extremity motor prostheses. *Crit Rev Biomed Eng* 16: 105–140, 1988.
50. **Robertson DG, Winter DA.** Mechanical energy generation, absorption and transfer amongst segments during walking. *J Biomech* 13: 845–854, 1980.
51. **Sadeghi H, Sadeghi S, Allard P, Labelle H, Duhaime M.** Lower limb muscle power relationships in bilateral able-bodied gait. *Am J Phys Med Rehabil* 80: 821–830, 2001.
52. **Samson W, Desroches G, Cheze L, Dumas R.** 3D joint dynamics analysis of healthy children's gait. *J Biomech* 42: 2447–2453, 2009.
53. **Schmalz T, Blumentritt S, Jarasch R.** Energy expenditure and biomechanical characteristics of lower limb amputee gait: the influence of prosthetic alignment and different prosthetic components. *Gait Posture* 16: 255–263, 2002.
54. **Schneider K, Hart T, Zernicke RF, Setoguchi Y, Oppenheim W.** Dynamics of below-knee child amputee gait: SACH foot versus Flex foot. *J Biomech* 26: 1191–1204, 1993.
55. **Segal AD, Orendurff MS, Klute GK, McDowell ML, Pecoraro JA, Shofer J, Czerniecki JM.** Kinematic and kinetic comparisons of transfemoral amputee gait using C-Leg and Mauch SNS prosthetic knees. *J Rehabil Res Dev* 43: 857–870, 2006.
56. **Simon AM, Hargrove LJ, Lock BA, Kuiken TA.** A strategy for minimizing the effect of misclassifications during real time pattern recognition myoelectric control. *Conf Proc IEEE Eng Med Biol Soc* 2009: 1327–1330, 2009.
57. **Sup F, Varol HA, Mitchell J, Withrow T, Goldfarb M.** Design and control of an active electrical knee and ankle prosthesis. *Proc IEEE RAS EMBS Int Conf Biomed Robot Biomechatron* 2008: 523–528, 2008.
58. **Winter DA.** Biomechanical motor patterns in normal walking. *J Mot Behav* 15: 302–330, 1983.
59. **Winter DA.** Energy generation and absorption at the ankle and knee during fast, natural, and slow cadences. *Clin Orthop Relat Res* 175: 147–154, 1983.
60. **Winter DA, Patla AE, Frank JS, Walt SE.** Biomechanical walking pattern changes in the fit and healthy elderly. *Phys Ther* 70: 340–347, 1990.
61. **Winter DA, Sienko SE.** Biomechanics of below-knee amputee gait. *J Biomech* 21: 361–367, 1988.
62. **Yang J, Jin D, Ji L, Wang R, Zhang J, Fang X, Zhou D, Wu M.** The reaction strategy of lower extremity muscles when slips occur to individuals with trans-femoral amputation. *J Electromyogr Kinesiol* 17: 228–240, 2007.
63. **Zwick EB, Saraph V, Linhart WE, Steinwender G.** Propulsive function during gait in diplegic children: evaluation after surgery for gait improvement. *J Pediatr Orthop B* 10: 226–233, 2001.